AJS American Journal of Science
publishing earth-sciences research since 1818

Zhao, M., Planavsky, N., Wang, X., Zhang, Y., & Hein, J. R. (2023). A Cenozoic Record of Deep Oceanic Zn Isotopic Composition in Ferromanganese Crusts. *American Journal of Science*, *323*, 10. https://doi.org/10.2475/001c.89628

Science Paper

A Cenozoic Record of Deep Oceanic Zn Isotopic Composition in Ferromanganese Crusts

Mingyu Zhao[1a], Noah Planavsky[2], Xiangli Wang[1], Yiyue Zhang[2], James R. Hein[3]

[1] Key Laboratory of Cenozoic Geology and Environment, Institute of Geology and Geophysics, Chinese Academy of Sciences, [2] Department of Earth and Planetary Sciences, Yale University, [3] PCMSC, United States Geological Survey

Keywords: Zinc isotope, Ferromanganese crusts, Cenozoic, Pacific Ocean, Carbon cycle

https://doi.org/10.2475/001c.89628

American Journal of Science

Vol. 323, 2023

The zinc (Zn) isotopic composition (δ^{66}Zn) of the deep ocean (>1000 m) can provide insights into the carbon cycle, the biological pump, and hydrothermal activity. However, we have an incomplete view of the temporal and spatial evolution of deep-ocean Zn isotopes. Here, we present new δ^{66}Zn values of Fe-Mn crusts from the Pacific Ocean, which we used to reconstruct the evolution of deep-ocean δ^{66}Zn for the Cenozoic. Our results suggest that the δ^{66}Zn values remain stable in the deep Pacific Ocean at around ~ 0.5‰ through the Cenozoic. Our results limit the extent of change in organic zinc burial through the Cenozoic. However, given uncertainties in the global mass balance and analytical error, variations of roughly 20% in organic zinc burial are still possible.

1. Introduction

Zinc is an essential nutrient strongly coupled with the marine organic carbon cycle. Zinc has the potential to limit marine primary productivity under certain conditions (Anderson et al., 1978; Moore et al., 2013; Morel et al., 1994; Shaked et al., 2006). The reversible scavenging of Zn onto organic matter and the downward transport of organic Zn are important processes of Zn cycling in ocean water (John & Conway, 2014; Weber et al., 2018). Further, the burial of Zn in marine sediments is likely linked to the extent of sulfide generated by sulfate reduction (Tribovillard et al., 2006). Therefore, the Zn concentration and isotopic compositions of ancient seawater recorded in marine sediments may provide vital information on the marine organic carbon cycle, which is a strong lever on climate and Earth's redox budget (e.g., Berner, 2004; Xiao et al., 2023; Zhao et al., 2023).

Dissolved δ^{66}Zn values of modern surface ocean waters (<1000 m) vary substantially from -1.1‰ to +0.9‰, probably due to isotopic fractionation related to biological uptake and adsorption on organic particles (Bermin et al., 2006; Conway & John, 2014, 2015; John et al., 2018; Lemaitre et al., 2020; Weber et al., 2018; Zhao et al., 2021). In contrast, the Zn isotopic composition in modern deep ocean (>1000 m) is relatively homogeneous with a mean δ^{66}Zn value of ~0.5‰ (Conway & John, 2014, 2015; John et al., 2018; Lemaitre et al., 2020). On the other hand, low δ^{66}Zn values (-0.2 to 0.2‰) can occur regionally in the deep ocean that is strongly influenced by hydrothermal fluids or diffusion flux from Zn-rich porewaters in sediments (Conway & John, 2014; John et al., 2018; Lemaitre et al., 2020). Rivers are the largest Zn source to the oceans, with δ^{66}Zn values in a narrow range of 0.19 to 0.56‰ (John et al., 2008; Little, Vance, et al., 2014). The two most important marine Zn burial fluxes are Fe-Mn oxides and organic-rich sediments along continental margins, with δ^{66}Zn in the ranges of 0.53 to 1.42‰ and -0.15 to 0.47‰, respectively (Little et al., 2016; Weber et al., 2018). Therefore, the Zn isotope composition of the deep marine waters has the potential to provide new insights into the evolution of the biological pump (the export of organic matter from surface waters into the ocean interior).

There have been limited attempts to reconstruct the evolution of deep-ocean δ^{66}Zn. So far, the only study from Fe-Mn crusts revealed relatively constant δ^{66}Zn values (1.06 to 1.23‰ for crust D11-1) during the last 20 Myr (Little, Vance, et al., 2014). Here, we provide further Zn concentration and isotopic measurements on two previously extensively studied Fe-Mn crusts (D11-1 and CD29-2) from the Pacific Ocean, in order to reconstruct the δ^{66}Zn composition of deep ocean for the last 90 Myr. We found that in the deep Pacific Ocean, the δ^{66}Zn remains relatively constant during the Cenozoic, which implies limited changes in the marine zinc cycle and, by inference, the biological pump.

a Corresponding author. Email: mingyu.zhao@mail.iggcas.ac.cn

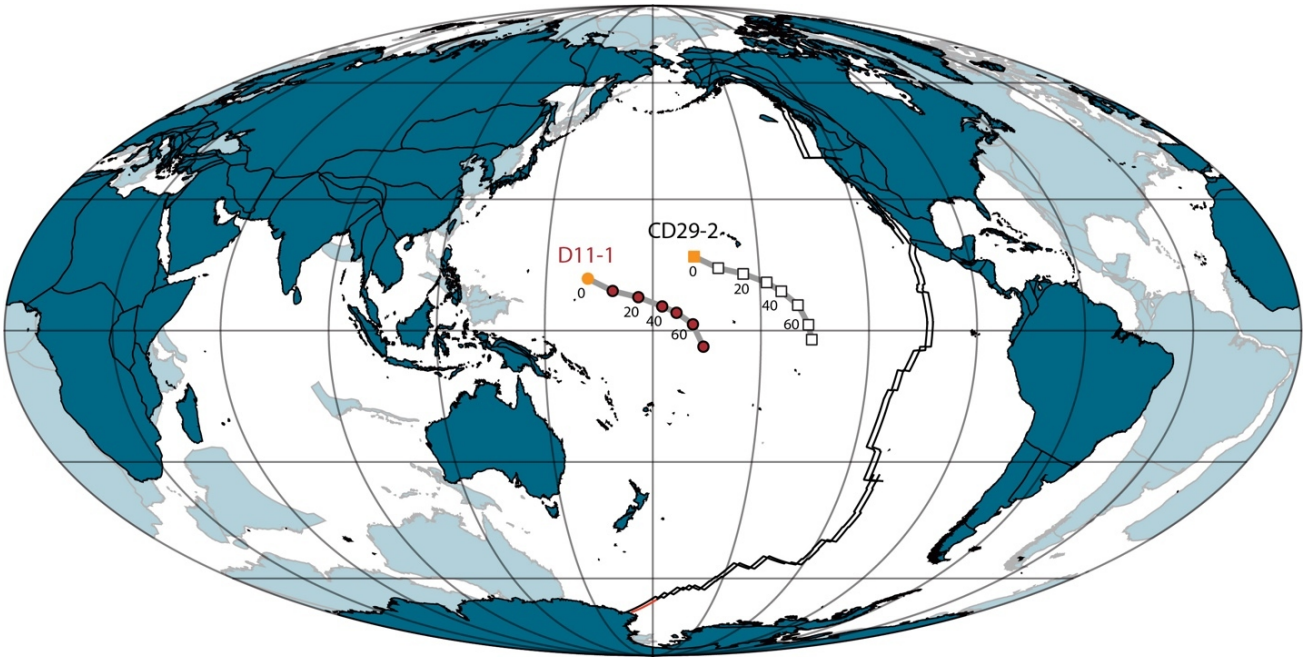

Figure 1. Paleotracks of crusts CD29-2 and D11-1. All reconstructions were made using GPlates software (Müller et al., 2018). Reconstruction model is from Matthews et al. (2016). The time interval between the dots is 10 Myrs. The numbers represent the ages of the locations in Ma. The black line is the current East Pacific Rise.

Table 1. A calculation on the effective diffusivity for Zn in the Fe-Mn crust.

Element	Seawater	Refs.	Fe-Mn crust	Relative K_c^X	D_{eff}^X
	ppm		ppm		cm^2/yr
Zn	9.15×10^{-5}	Conway and John (2014)	100	1.09×10^{6}	4.67×10^{-9}
Os	1.10×10^{-5}	Henderson and Burton (1999)	0.00183	$1.70E\times10^{2}$	3.0×10^{-5}

Note: the calculation follows the method described in Henderson and Burton (1999).

2. Materials and Methods

2.1. Samples

Two Fe-Mn crusts (D11-1 and CD29-2) from the Pacific Ocean (fig. 1) were investigated in this study. Crusts D11-1 and CD29-2 come from seamounts at water depths of 1690–1870 and 1970–2390 m, respectively (Christensen et al., 1997). Detailed information on the locations and the mineralogy of these two sites is provided in Christensen et al. (1997) and Ling et al. (1997). Samples at every 2 mm interval were drilled from the crusts. The age model of crust CD29-2 comes from Klemm et al. (2005), which was calibrated using the well-known marine Os isotopic evolution of the past 80 Ma. The age model of the crust D11-1 comes from Nielsen et al. (2009), which is also based on the Os isotope stratigraphy and shows a good match between crusts CD29-2 and D11-1. Based on the age models of the two sites, the each 2-mm sampling interval represents 1–2 Myr. Further, the presence of well-defined Os isotope variations rules out the presence of total diffusional overprinting of Zn isotope signature, as Os diffuses ~6000 times quicker than Zn (table 1).

2.2. Analytical method

An extended x-ray absorption fine structure (EXAFS) study indicates that Zn is mainly associated with birnessite (δ-MnO_2) in the Fe-Mn crusts (Little, Sherman, et al., 2014). Thus, 10 mL 0.1M NH_2OH-HCl solution was used to selectively dissolve Mn oxides in ~5 mg drilled samples (Neaman et al., 2004), which can avoid significant contamination from iron oxides and other minerals. About 5 mg drilled samples were dissolved in 10 mL 0.1M NH_2OH-HCl solution for 2 days after ultrasonic vibration for 2–3 h. After centrifugation, the solutions were dried down and re-dissolved in 6N HCl.

A small portion of the solution was used for element analysis (including Zn and Mn) on a Thermo Element-XR inductively coupled plasma mass spectrometry (ICP-MS) at the Yale University Metal Geochemistry Center (Zhao et al., 2021). The solutions were further purified using anion-exchange resin AG MP-1 (100–200 mesh), following the protocols described by Isson et al. (2018) and Zhao et al. (2021). The Zn isotopic composition of purified samples with 100 ppb Zn in 5 % HNO_3 were measured on a Thermo Finnigan Neptune Plus MC-ICP-MS at the Yale University Metal Geochemistry Center. One or two overall procedural

Table 2. Zn isotopic results of the standards

Standard	$\delta^{66}Zn$ ‰	Standard	$\delta^{66}Zn$ ‰
Nod-P-1	0.85	IRMM	0.31
Nod-P-1	0.84	IRMM	0.36
Nod-P-1	0.83	IRMM	0.33
Nod-P-1	0.87	IRMM	0.37
Average	0.85	IRMM	0.34
2SD	0.03	IRMM	0.39
		IRMM	0.32
		IRMM	0.37
		IRMM	0.34
		IRMM	0.30
		IRMM	0.30
		IRMM	0.36
		IRMM	0.35
		IRMM	0.37
		IRMM	0.33
		IRMM	0.32
		IRMM	0.32
		IRMM	0.38
		IRMM	0.34
		IRMM	0.33
		IRMM	0.32
		IRMM	0.32
		IRMM	0.33
		IRMM	0.34
		IRMM	0.31
		IRMM	0.33
		IRMM	0.38
		IRMM	0.32
		IRMM	0.31
		IRMM	0.32
		IRMM	0.33
		IRMM	0.32
		IRMM	0.31
		IRMM	0.33
		IRMM	0.31
		IRMM	0.32
		Average	0.33
		2SD	0.05

blanks were run for each batch, with the Zn concentrations <1% of the samples. Zn isotope data are reported here relative to the standard JMC Lyon using delta notation. The external precision for Zn isotopic analysis is better than ± 0.05 ‰ (2σ), based on the repeated analyses of standards IRMM ($\delta^{66}Zn$=0.33±0.05‰, n=38) and Nod-P-1 ($\delta^{66}Zn$=0.85±0.03‰, n=4) (table 2). More detailed methods and information on Neptune operating conditions are given in Isson et al. (2018) and Zhao et al. (2021).

We have used 0.1M NH_2OH-HCl solution to target only Mn oxides, in order to preclude significant contamination from iron oxides and other minerals (Neaman et al., 2004). The $\delta^{66}Zn$ measured using this method is slightly higher (~0.1‰) than the results of Little, Vance et al. (2014) for the same crust D11-1 (figs. 2 and 3, and table 3), where 0.4M HCl was used to digest the samples. To compare with the results of Little, Vance et al. (2014), we have digested four samples using 6M HCl. As shown in figure 2, the results us-

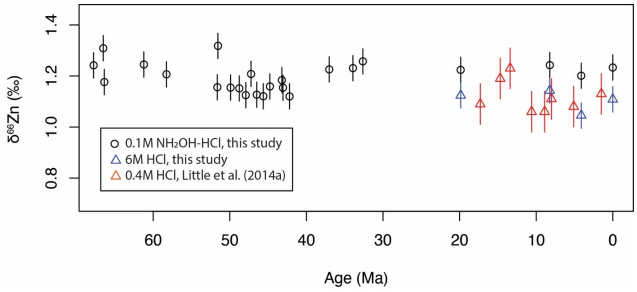

Figure 2. $\delta^{66}Zn$ results of Fe-Mn crust D11-1 generated by different digestion methods. The $\delta^{66}Zn$ results of the four samples digested using 6M HCl (with ages of 0, 4.11, 8.23 and 19.85 Ma) are 1.11, 1.05, 1.14 and 1.12 ‰, respectively. The error bars represent the analytical errors (2σ).

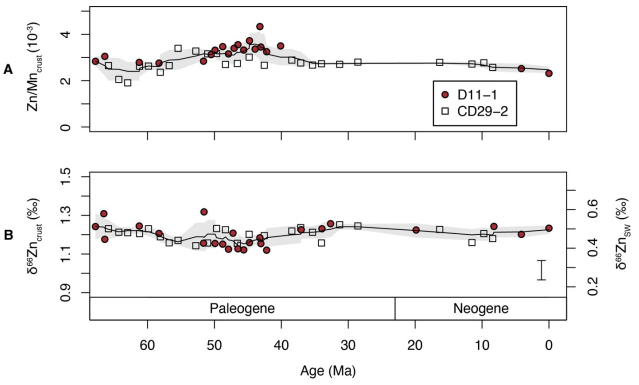

Figure 3. $\delta^{66}Zn$ and Zn/Mn results from the two Fe-Mn crusts and the calculated seawater $\delta^{66}Zn$. Lines represent results of 5 points moving average. The shadows represent standard deviations during moving average analysis. The error bar represents the analytical error (2σ).

ing 6M HCl compare well with the results of Little, Vance et al. (2014). This thus indicates that our analytical results are robust. The ~0.1‰ higher $\delta^{66}Zn$ values of Fe-Mn crusts digested using 0.1M NH_2OH-HCl solution likely results from less contamination from detrital materials and iron oxides. The detrital materials have a lower $\delta^{66}Zn$ of ~0.3‰ (Little, Vance, et al., 2014), much lower than that of the Mn oxides (~1.2‰). It was also found that the adsorption of Zn to Fe oxides results in smaller fractionations than Mn oxides (Bryan et al., 2015; Juillot et al., 2008), with $\Delta^{66}Zn_{adsorbed\text{-}aqueous}$=+0.29‰ for goethite and $\Delta^{66}Zn_{adsorbed\text{-}aqueous}$=+0.53‰ for ferrihydrite.

2.3. The global mass-balance model

In order to understand variation of Zn cycle and perhaps biological pump during the Cenozoic, we built a simple global mass-balance model to simulate the variations of $\delta^{66}Zn$ of seawater ($\delta^{66}Zn_{sw}$). In this simple model, the Zn flux from land to seawater through river and aerosol dust are lumped together into one term F_{in} (fig. 4). Following the previous studies (e.g., Isson et al., 2018; Little, Vance, et al., 2014), three Zn burial fluxes are included, which are Zn burial flux related to Fe-Mn crusts (B_{ox}), Zn burial flux in organic-rich sediments (B_{org}) and Zn burial flux associated with carbonate and silica (B_{other}).

The proportion of marine Zn burial in organic-rich sediments relative to the sum of Zn burial in the ocean (f_{org_Zn}) is calculated as:

$$f_{org\_Zn} = \frac{B_{org}}{B_{org} + B_{ox} + B_{other}} = \frac{B_{org}}{F_{in}} \quad (1)$$

Similarly, the proportion of marine Zn burial in carbonate and silica relative to the sum of Zn burial in the ocean (f_{other}) is calculated using:

$$f_{other} = \frac{B_{other}}{B_{org} + B_{ox} + B_{other}} = \frac{B_{other}}{F_{in}} \quad (2)$$

The main equation for the time evolution of $\delta^{66}Zn_{sw}$ is:

$$\begin{aligned} \frac{d\delta^{66}Zn_{sw}}{dt} &= \frac{F_{in} * \delta^{66}Zn_{in} - B_{ox} * (\delta^{66}Zn_{sw} + \Delta_{ox}) - B_{org} * (\delta^{66}Zn_{sw} + \Delta_{org}) - B_{other} * \delta^{66}Zn_{sw}}{Zn_{sw0} * V} \\ &= [F_{in} * \delta^{66}Zn_{in} - F_{in} * (1 - f_{org\_Zn} - f_{other}) * (\delta^{66}Zn_{sw} + \Delta_{ox}) \\ &\quad - F_{in} * f_{org\_Zn} * (\delta^{66}Zn_{sw} + \Delta_{org}) - F_{in} * f_{other} * \delta^{66}Zn_{sw}] / (Zn_{sw0} * V) \end{aligned} \quad (3)$$

where $\delta^{66}Zn_{in}$ is $\delta^{66}Zn$ of Zn sources to seawater, Δ_{ox} is the Zn isotopic fractionation between Fe-Mn crusts and seawater, Δ_{org} is the Zn isotopic fractionation between organic-rich sediments and seawater, and V is the total volume of seawater. Zn_{sw0} represents the Zn concentration of modern ocean water, assuming that Zn concentration of deep ocean hasn't change much throughout the Cenozoic, which is likely supported by the Zn/Mn data of this study. The values and ranges of each parameter can be found in table 4.

In modern ocean, the Zn burial flux associated with carbonate and silica is small relative to Zn burial associated with Fe-Mn crust and organic-rich sediments (table 4). Thus, for simplification, B_{other} and thus f_{other} are fixed terms in the simulation of the Cenozoic Zn cycle. Following the previous finding on shallow-water carbonate (Zhao et al., 2021), no Zn isotopic fractionation is applied between carbonate/silica and seawater. The $\delta^{66}Zn$ of organic-rich sediments in continental margin have a large range (-0.1 to 0.7‰, Horner et al., 2021; Little et al., 2016; Weber et al., 2018; Zhang et al., 2021). Thus, there is a large uncertainty in the estimation of the average Δ_{org} in the global ocean, which could be in the range of -0.41 to -0.15‰ (Isson et al., 2018; Little et al., 2016; Weber et al., 2018). Similarly, there is also a considerable variation in Δ_{ox} among different sites (Bryan et al., 2015; Maréchal et al., 2000; Pokrovsky et al., 2005; this study), which is commonly in the range of 0.4 to 0.7‰. The average $\delta^{66}Zn$ of Zn fluxes to seawater ($\delta^{66}Zn_{in}$) was estimated to be 0.33‰ (Little, Vance, et al., 2014). $\delta^{66}Zn_{in}$ and F_{in} may have varied throughout the Cenozoic, which may have contributed to the variation in the $\delta^{66}Zn$ of the Fe-Mn crusts observed in this study. However, these two terms are also fixed in the current simulation, as their variations during the Cenozoic are largely unknown. We further estimate the maximum possible change in f_{org_Zn} during the Cenozoic under fixed $\delta^{66}Zn_{in}$ and F_{in}. With the constraints discussed above, it is thus possible to calculate the relationship between $\delta^{66}Zn_{sw}$ and f_{org_Zn} under different Δ_{org} and Δ_{ox} through running the model to steady state, which can further be used to estimate f_{org_Zn} using the $\delta^{66}Zn_{sw}$ val-

Table 3. The geochemical results of the two Fe-Mn crusts.

CD29-2						
Age	Depth	$\delta^{66}Zn$	Zn/Mn	Al	Zn	P
Ma	mm	‰		ppm	ppm	ppm
8.4	19	1.18	0.00257	1277	428	59
9.7	23	1.21	0.00277	1803	421	103
11.5	26	1.16	0.00272	1835	381	53
16.3	29	1.23	0.00279	1470	470	111
28.6	33	1.25	0.00280	1210	496	129
31.3	36	1.25	0.00270	1341	516	148
34.0	39	1.16	0.00273	1071	458	78
35.3	42	1.21	0.00267	1326	393	167
37.1	46	1.24	0.00277	1457	390	5397
38.4	49	1.22	0.00289	1249	367	17614
42.6	52	1.20	0.00266	1098	285	16449
44.8	55	1.20	0.00301	1280	245	14779
46.6	59	1.16	0.00274	998	204	11950
48.4	63	1.23	0.00270	1042	264	16434
49.7	66	1.23	0.00317	869	327	16263
51.0	69	1.16	0.00316	1014	374	18089
52.8	73	1.14	0.00328	944	230	27059
55.4	79	1.17	0.00340	1191	576	10008
56.8	82	1.16	0.00265	1093	492	9684
58.1	85	1.19	0.00236	824	366	3886
59.9	89	1.23	0.00263	851	388	3729
61.2	92	1.21	0.00262	935	552	5407
63.0	96	1.21	0.00191	789	333	4183
64.3	99	1.21	0.00205	1076	367	5293
65.8	103	1.23	0.00265	1275	386	6907
67.2	106	1.30	0.00192	934	331	5198
D11-1						
Age	Depth	$\delta^{66}Zn$	Zn/Mn	Al	Zn	P
Ma	mm	‰		ppm	ppm	ppm
0.0	0	1.23	0.00231	1647	481	721
4.1	8	1.20	0.00252	2027	391	355
8.2	17	1.24	NA	NA	NA	NA
19.9	35	1.22	NA	NA	NA	NA
30.0	50	NA	NA	NA	NA	NA
32.6	55	1.26	NA	NA	NA	NA
33.9	60	1.23	NA	NA	NA	NA
37.0	71	1.23	NA	NA	NA	NA
40.1	82	NA	0.00350	1118	397	60333
42.2	89	1.12	0.00325	1277	367	34606
43.1	92	1.15	0.00345	1393	352	39035
43.2	93	1.18	0.00434	1562	416	53903
43.9	95	NA	0.00336	1143	289	42568
44.8	98	1.16	0.00372	1522	397	25550
45.6	101	1.12	0.00332	1116	311	36786
46.5	104	1.13	0.00355	1330	333	30067

47.1	106	NA	0.00340	1452	377	31302
47.2	107	1.21	NA	NA	NA	NA
47.9	109	1.12	0.00316	1090	286	41446
48.8	112	1.15	0.00347	1141	372	35122
49.9	116	1.15	0.00332	1262	528	30767
50.5	118	NA	0.00312	1065	535	20026
51.6	122	1.32	NA	NA	NA	NA
51.6	122	1.16	0.00284	1375	653	30855
58.3	131	1.21	0.00276	1632	521	22773
61.2	135	1.24	0.00279	1281	400	20510
66.4	142	1.18	0.00305	1776	719	5604
66.5	142	1.31	NA	NA	NA	NA
67.8	145	1.24	0.00283	2129	576	15275

Note: "NA" represents "not analyzed".

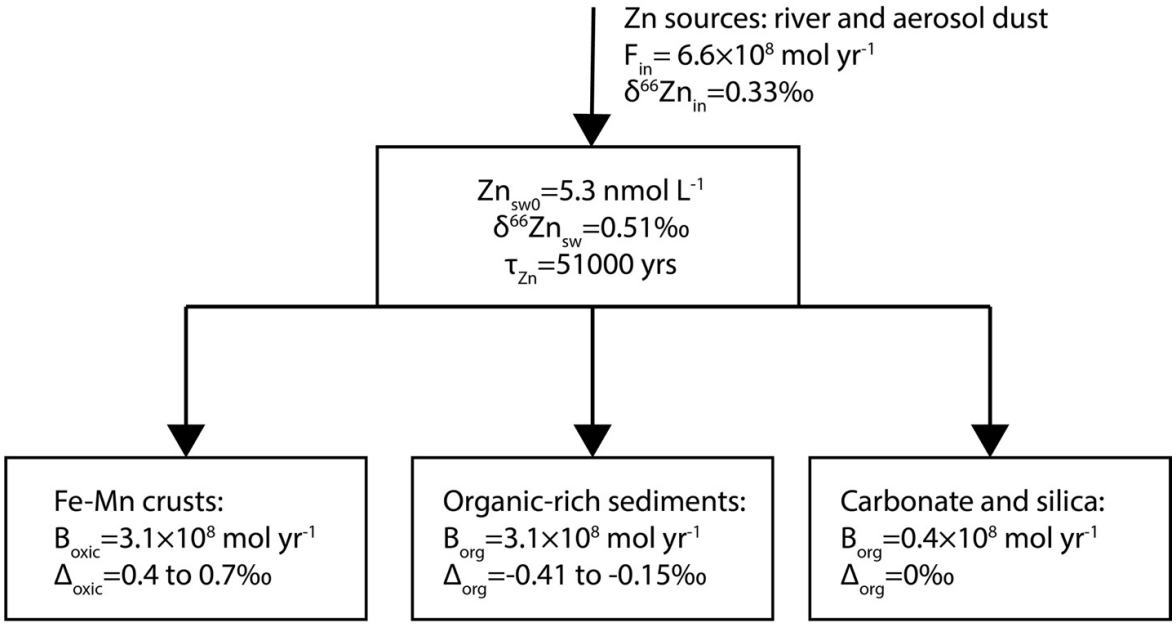

Figure 4. A schematic diagram for modern Zn budget.

ues inferred from the record of the Fe-Mn crusts. The calculated relationships between $\delta^{66}Zn_{sw}$ and f_{org_Zn} are shown as figure 5.

3. Results

The measured Zn/Mn ratios are in the range of 1.9×10^{-3} to 4.3×10^{-3} (fig. 3 and table 3). We use Zn/Mn because much of the Zn in Fe-Mn crusts (61-83%) is shown to be associated with the Mn phase (Koschinsky & Hein, 2003) and the NH_2OH-HCl used during digestion only attacks Mn oxides (Neaman et al., 2004). Measured $\delta^{66}Zn$ values of the Fe-Mn crusts range from 1.12‰ to 1.32‰ (fig. 3 and table 3). The two measured crusts D11-1 and CD29-2 have similar Zn/Mn and $\delta^{66}Zn$ values (fig. 3). Zn/Mn shows a small increase from ~2.5×10^{-3} to ~3.5×10^{-3} from 62 Ma to 43Ma, followed by a gradual decrease from ~3.5×10^{-3} to ~2.5×10^{-3} from 43 Ma to the present. $\delta^{66}Zn$ is stable around 1.2‰ throughout the Cenozoic. The magnitude of variation in $\delta^{66}Zn$ (±0.1‰) is slightly larger than the analytical error (±0.05‰, 2σ). The measured $\delta^{66}Zn$ values for the last 20 Myrs is ~0.1‰ higher than the previous measured values of crust D11-1 (fig. 2, Little, Vance, et al., 2014). However, as discussed earlier, this offset can be linked to different digestion solution (0.1M NH_2OH-HCl) from that of Little, Vance et al. (2014) (0.4M HCl). Stronger acid digests yield values similar to those reported by Little, Vance et al. (2014), perhaps due the attack of stronger acid on some silicate minerals (fig. 2). Zn and Al concentrations show no obvious correlation both crusts D11-1 (R^2=0.21, n=20) and CD29-2 (R^2=0.06, n=26; fig. S1).

Table 4. Values of parameters used in the model

Parameters	Descriptions	Values	References
F_{in}	Zn sources (predominantly riverine and aerosol dust) to seawater	6.6×10^{8} mol yr^{-1}	Gaillardet et al. (2003); Little, Vance et al. (2014)
B_{other}	Rate constant of Zn burial related to carbonate and silica	0.4×10^{8} mol yr^{-1}	Little, Vance et al. (2014)
f_{other}	Proportion of marine Zn burial in carbonate and silica relative to the sum of Zn burial in the ocean	6%	Little, Vance et al. (2014)
Zn_{sw0}	Zn concentration of modern ocean water	5.3 nM	Chester (2009)
V	Volume of seawater	1.37×10^{21} L	Charette and Smith (2010)
$\delta^{66}Zn_{in}$	δ^{66}Zn of Zn sources to seawater	0.33‰	Little, Vance et al. (2014)
Δ_{ox} [a]	Zn isotopic fractionation between Fe-Mn crusts and seawater	0.4 to 0.7‰	Maréchal et al. (2000); Pokrovsky et al. (2005); Bryan et al. (2015); This study
Δ_{org} [b]	Zn isotopic fractionation between organic-rich sediments and seawater	-0.15 to -0.41‰	Little et al. (2016); Isson et al. (2018); Weber et al. (2018)

Note: a. This value is allowed to vary in the model. Note that the Δ_{ox} applied in the mass balance model is a global average value for both Fe and Mn oxides. This is different from the site-special Δ_{ox} (fixed as 0.7‰) to calculate seawater δ^{66}Zn compositions from the δ^{66}Zn values of Mn oxides in Fe-Mn crusts of this study.
b. This value is allowed to vary in the model.

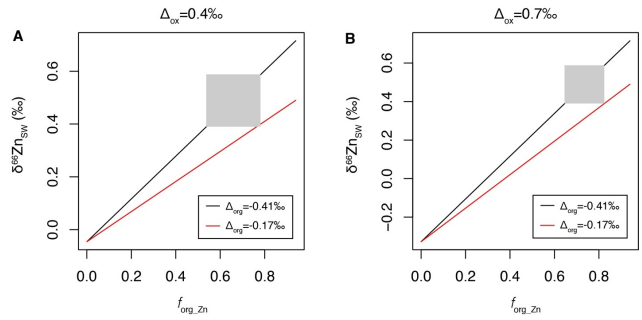

Figure 5. Results of the mass balance model of global Zn cycle. $f_{org\text{-}Zn}$ represents the proportation of marine Zn burial in organic-rich sediments relative to the sum of Zn burial ($f_{org\text{-}Zn}=B_{org}/(B_{ox}+B_{org}+B_{other})$). The shadows represent the range of variation inferred from the δ^{66}Zn results of Fe-Mn crusts in this study.

4. Discussion

4.1 The evolution of seawater Zn isotopic composition

Seafloor Fe-Mn crusts have been extensively used as an archive for the seawater chemistry as they directly precipitate from seawater (e.g., Christensen et al., 1997; Klemm et al., 2005; Ling et al., 1997; Little, Vance, et al., 2014; Nielsen et al., 2009; Wang et al., 2016). Our measured δ^{66}Zn values of the Cenozoic Fe-Mn crusts (~1.2‰) are consistent with the previous finding that Zn isotopic compositions of the Fe-Mn crusts are 0.5–0.7‰ higher than that of dissolved Zn in deep oceanic water (Boyle et al., 2012; Little, Sherman, et al., 2014; Little, Vance, et al., 2014). The lack of strong correlations between Zn and Al (R^2=0.06 and 0.21 for crust D11-1 and CD29-2, respectively), suggests that the variations in δ^{66}Zn and Zn/Mn do not reflect contamination from detrital minerals. Phosphorus concentration results indicate the occurrence of phosphatization only in the >30 Ma part of the crust D11-1 and CD29-2 (Ling et al., 1997). This is also supported by the measured P concentration in this study, which shows a significant shift in P concentration around 30 Ma (table 3). However, there are no obvious changes in δ^{66}Zn and Zn/Mn around 30 Ma, consistent with a limited influence of phosphatization on the δ^{66}Zn and Zn/Mn of the crusts. Therefore, there is strong basis for linking δ^{66}Zn values of Fe-Mn crusts to seawater composition. The variations in Zn/Mn of the Fe-Mn crusts may reflect a change in seawater Zn concentration or the environmental forcings (such as *p*H, redox state and temperature etc.) that could have an influence on the adsorption of Zn by Mn oxides (birnessite, Little, Sherman, et al., 2014). Following Little, Vance, et al., 2014, the δ^{66}Zn values of seawater ($\delta^{66}Zn_{SW}$) were calculated with an application of 0.7‰ offset between Mn oxides in Fe-Mn crusts and seawater (fig. 3). This offset is applied because the δ^{66}Zn value of the youngest sample of crust D11-1 at 0.0 Ma shows a value of 1.23‰ (table 3), which is ~0.7‰ higher than that of modern deep ocean water (~0.5‰). This offset is also consistent with the previous estimates based on modern Fe-Mn crusts (e.g., Little, Vance, et al., 2014; Maréchal et al., 2000).

In the modern ocean, deep-water $\delta^{66}Zn_{SW}$ (>1000 m) is generally homogeneous, with a mean value of ~0.4‰ to 0.5‰ (Conway & John, 2014, 2015; John et al., 2018; Lemaitre et al., 2020). The distance between the two studied Fe-Mn crusts is about 4000 km (fig. 1), with water depths of ~2000 m. Eruption and/or erosion of the seamount must had ceased before the continuous growth of the Fe-Mn crusts on it (Meynadier et al., 2008). Thus, these processes won't have much influence on the long-term variations of water depths of the studied Fe-Mn crusts. However, due to the subsidence of oceanic crust with distance from the ridge, the studied two sites were likely shallower in the past.

The relatively constant $\delta^{66}Zn_{SW}$ since ~67 Ma suggest that the large part of the deep Pacific Ocean near the study

sites has homogeneous $\delta^{66}Zn_{SW}$ of ~0.5‰ during this period, which is the same, within analytical error, as modern deep-ocean waters. Previous measurements on Fe-Mn crusts of the Atlantic and Indian oceans also show limited variation of $\delta^{66}Zn$ in Fe-Mn crusts (~1‰) during the last 20 Myrs (fig. S2, Little, Vance, et al., 2014). The $\delta^{66}Zn$ of Fe-Mn crusts of the Atlantic is ~0.1‰ lower than that of the Pacific (Little, Vance, et al., 2014), and whether this reflects changes in fractionation or deep seawater composition requires further investigation.

4.2 Implication for the evolution of organic Zn burial and biological pump

Zinc isotope compositions of ocean-water profiles are controlled by uptake and sorption of Zn and the interplay of those processes—likely along with fractionation during sulfide formation resulting in burial of isotopically light Zn in high productivity settings (Little et al., 2016; Weber et al., 2018). Although the $\delta^{66}Zn$ of organic-rich sediments in continental margins have a large range (-0.1 to 0.7‰, Horner et al., 2021; Little et al., 2016; Weber et al., 2018; Zhang et al., 2021), the average $\delta^{66}Zn$ of authigenic Zn in organic-rich sediments (0.1 to 0.35‰, Isson et al., 2018; Little et al., 2016; Weber et al., 2018) is likely lower than that of seawater (~0.5‰). This is also supported by a simple Zn isotopic mass balance model, which requires a major Zn sink with $\delta^{66}Zn$ lower than that of the Zn sources to seawater (0.33‰, Little, Vance, et al., 2014). Intriguingly, our record suggests the suite of processes controlling the Zn cycle have no fundamental change over the entire Cenozoic despite a large change in ocean temperatures and marine ecosystems (e.g., Norris et al., 2013; Zachos et al., 2001), which is typically envisioned to have changed the operation of the biological pump (e.g., Boscolo-Galazzo et al., 2021; Fakhraee et al., 2020).

We have used a simple mass balance model to understand the implication of the $\delta^{66}Zn$ results of Fe-Mn crusts on the evolution of global Zn cycle throughout the Cenozoic (figs. 4 and 5), assuming that the $\delta^{66}Zn$ variations (1.12‰ to 1.32‰) of the Fe-Mn crusts only reflect variations in $\delta^{66}Zn$ of deep ocean water and perturbations in global Zn cycle. This allows us to estimate the maximum possible perturbation of global Zn cycle during the Cenozoic, as other factors such as local ocean water conditions and Zn speciation may also have some contribution to the $\delta^{66}Zn$ variations (1.12‰ to 1.32‰) of the Fe-Mn crust. For example, in the normal *p*H range of ocean water (7–8.2), changes in Zn speciation can have a small influence (<0.1‰) on the $\delta^{66}Zn$ of free Zn^{2+} that can be adsorbed by Fe-Mn crusts (e.g., Mavromatis et al., 2019).

Using a simple mass balance model for global Zn cycle, we have calculated the possible proportation of marine Zn burial in organic-rich sediments relative to the sum of Zn burial (f_{org_Zn}) that could explain the $\delta^{66}Zn$ results in this study (fig. 5). In the situation of Δ_{ox}= 0.4‰ and Δ_{org}= -0.41‰, a f_{org_Zn} variation in the range of 0.54 to 0.78 would be required to explain the range of $\delta^{66}Zn_{sw}$ inferred from the results of Fe-Mn crusts. The required f_{org_Zn} would be in the range of 0.65 to 0.82, when Δ_{ox}= 0.7‰ and Δ_{org}= -0.41‰. However, under Δ_{org}= -0.17‰, it is not possible to explain the highest $\delta^{66}Zn_{sw}$ inferred from the results of Fe-Mn crusts (0.59‰) even if f_{org_Zn} =0.94, which means that there is no Zn burial with Fe-Mn crusts. Thus, Δ_{org}= -0.17‰ is not a possible situation under current model framework. Thus, our results limit the extent of change in organic zinc burial through the Cenozoic. However, given uncertainties in the global mass balance and analytical error, variations of roughly 20% in organic zinc burial (i.e., a range of f_{org_Zn} from 0.65 to 0.82 when Δ_{org}= -0.41‰) are still possible.

5. Conclusions

Our $\delta^{66}Zn$ results from two central Pacific Fe-Mn crusts suggest that the $\delta^{66}Zn$ values of Pacific Ocean deep water remained stable around ~0.5‰ through the entire Cenozoic. Using a simple mass balance model of global Zn cycle, we can constrain the evolution of organic Zn burial during the Cenozoic. Considering the uncertainties in the global mass balance and analytical error, our model results show that variations of ~20% in organic zinc burial through the Cenozoic are still possible.

Acknowledgments

We greatly thank Dan Asael for his help in the lab work and Zheng Gong for his help on the tectonic maps. M.Z. is funded by the programme of the Chinese Academy of Sciences (E251520401) and the IGGCAS Key programme (no. IGGCAS-202201). We thank two anonymous reviewers for critical feedback that improved this manuscript.

Data Availability

https://data.mendeley.com/datasets/h4nrs68zvy/1

Editor: C. Page Chamberlain, Associate Editor: Timothy W. Lyons

Submitted: January 04, 2023 EST, Accepted: October 26, 2023 EST

References

Anderson, M. A., Morel, F. M. M., & Guillard, R. R. L. (1978). Growth limitation of a coastal diatom by low zinc ion activity. *Nature*, *276*(5683), 70–71. https://doi.org/10.1038/276070a0

Bermin, J., Vance, D., Archer, C., & Statham, P. J. (2006). The determination of the isotopic composition of Cu and Zn in seawater. *Chemical Geology*, *226*(3–4), 280–297. https://doi.org/10.1016/j.chemgeo.2005.09.025

Berner, R. A. (2004). *The Phanerozoic carbon cycle: CO2 and O2*. Oxford University Press. https://doi.org/10.1093/oso/9780195173338.001.0001

Boscolo-Galazzo, F., Crichton, K. A., Ridgwell, A., Mawbey, E. M., Wade, B. S., & Pearson, P. N. (2021). Temperature controls carbon cycling and biological evolution in the ocean twilight zone. *Science*, *371*(6534), 1148–1152. https://doi.org/10.1126/science.abb6643

Boyle, E. A., John, S., Abouchami, W., Adkins, J. F., Echegoyen-Sanz, Y., Ellwood, M., Flegal, A. R., Fornace, K., Gallon, C., Galer, S., Gault-Ringold, M., Lacan, F., Radic, A., Rehkamper, M., Rouxel, O., Sohrin, Y., Stirling, C., Thompson, C., Vance, D., … Zhao, Y. (2012). GEOTRACES IC1 (BATS) contamination-prone trace element isotopes Cd, Fe, Pb, Zn, Cu, and Mo intercalibration: GT IC1 contamination-prone trace element isotopes. *Limnology and Oceanography: Methods*, *10*(9), 653–665. https://doi.org/10.4319/lom.2012.10.653

Bryan, A. L., Dong, S., Wilkes, E. B., & Wasylenki, L. E. (2015). Zinc isotope fractionation during adsorption onto Mn oxyhydroxide at low and high ionic strength. *Geochimica et Cosmochimica Acta*, *157*, 182–197. https://doi.org/10.1016/j.gca.2015.01.026

Charette, M. A., & Smith, W. H. F. (2010). The volume of Earth's ocean. *Oceanography*, *23*(2), 112–114. https://doi.org/10.5670/oceanog.2010.51

Chester, R. (2009). *Marine geochemistry* (2nd ed.). John Wiley & Sons.

Christensen, J. N., Halliday, A. N., Godfrey, L. V., Hein, J. R., & Rea, D. K. (1997). Climate and ocean dynamics and the lead isotopic records in Pacific ferromanganese crusts. *Science*, *277*(5328), 913–918. https://doi.org/10.1126/science.277.5328.913

Conway, T. M., & John, S. G. (2014). The biogeochemical cycling of zinc and zinc isotopes in the North Atlantic Ocean. *Global Biogeochemical Cycles*, *28*(10), 1111–1128. https://doi.org/10.1002/2014gb004862

Conway, T. M., & John, S. G. (2015). The cycling of iron, zinc and cadmium in the North East Pacific Ocean – Insights from stable isotopes. *Geochimica et Cosmochimica Acta*, *164*, 262–283. https://doi.org/10.1016/j.gca.2015.05.023

Fakhraee, M., Planavsky, N. J., & Reinhard, C. T. (2020). The role of environmental factors in the long-term evolution of the marine biological pump. *Nature Geoscience*, *13*(12), 812–816. https://doi.org/10.1038/s41561-020-00660-6

Gaillardet, J., Viers, J., & Dupré, B. (2003). Trace elements in river waters. *Treatise on Geochemistry*, *5*, 225–272. https://doi.org/10.1016/b0-08-043751-6/05165-3

Henderson, G. M., & Burton, K. W. (1999). Using (234U/238U) to assess diffusion rates of isotope tracers in ferromanganese crusts. *Earth and Planetary Science Letters*, *170*(3), 169–179. https://doi.org/10.1016/s0012-821x(99)00104-1

Horner, T. J., Little, S. H., Conway, T. M., Farmer, J. R., Hertzberg, J. E., Janssen, D. J., Lough, A. J. M., McKay, J. L., Tessin, A., Galer, S. J. G., Jaccard, S. L., Lacan, F., Paytan, A., Wuttig, K., & GEOTRACES-PAGES Biological Productivity Working Group Members. (2021). Bioactive Trace Metals and Their Isotopes as Paleoproductivity Proxies: An Assessment Using GEOTRACES-Era Data. *Global Biogeochemical Cycles*, *35*(11), e2020GB006814. https://doi.org/10.1029/2020gb006814

Isson, T. T., Love, G. D., Dupont, C. L., Reinhard, C. T., Zumberge, A. J., Asael, D., Gueguen, B., McCrow, J., Gill, B. C., Owens, J., Rainbird, R. H., Rooney, A. D., Zhao, M.-Y., Stueeken, E. E., Konhauser, K. O., John, S. G., Lyons, T. W., & Planavsky, N. J. (2018). Tracking the rise of eukaryotes to ecological dominance with zinc isotopes. *Geobiology*, *16*(4), 341–352. https://doi.org/10.1111/gbi.12289

John, S. G., & Conway, T. M. (2014). A role for scavenging in the marine biogeochemical cycling of zinc and zinc isotopes. *Earth and Planetary Science Letters*, *394*, 159–167. https://doi.org/10.1016/j.epsl.2014.02.053

John, S. G., Helgoe, J., & Townsend, E. (2018). Biogeochemical cycling of Zn and Cd and their stable isotopes in the Eastern Tropical South Pacific. *Marine Chemistry*, *201*, 256–262. https://doi.org/10.1016/j.marchem.2017.06.001

John, S. G., Rouxel, O. J., Craddock, P. R., Engwall, A. M., & Boyle, E. A. (2008). Zinc stable isotopes in seafloor hydrothermal vent fluids and chimneys. *Earth and Planetary Science Letters*, *269*(1–2), 17–28. https://doi.org/10.1016/j.epsl.2007.12.011

Juillot, F., Maréchal, C., Ponthieu, M., Cacaly, S., Morin, G., Benedetti, M., Hazemann, J. L., Proux, O., & Guyot, F. (2008). Zn isotopic fractionation caused by sorption on goethite and 2-Lines ferrihydrite. *Geochimica et Cosmochimica Acta*, *72*(19), 4886–4900. https://doi.org/10.1016/j.gca.2008.07.007

Klemm, V., Levasseur, S., Frank, M., Hein, J. R., & Halliday, A. N. (2005). Osmium isotope stratigraphy of a marine ferromanganese crust. *Earth and Planetary Science Letters*, *238*(1–2), 42–48. https://doi.org/10.1016/j.epsl.2005.07.016

Koschinsky, A., & Hein, J. R. (2003). Uptake of elements from seawater by ferromanganese crusts: solid-phase associations and seawater speciation. *Marine Geology*, *198*(3–4), 331–351. https://doi.org/10.1016/s0025-3227(03)00122-1

Lemaitre, N., de Souza, G. F., Archer, C., Wang, R.-M., Planquette, H., Sarthou, G., & Vance, D. (2020). Pervasive sources of isotopically light zinc in the North Atlantic Ocean. *Earth and Planetary Science Letters*, *539*, 116216. https://doi.org/10.1016/j.epsl.2020.116216

Ling, H. F., Burton, K. W., O'Nions, R. K., Kamber, B. S., von Blanckenburg, F., Gibb, A. J., & Hein, J. R. (1997). Evolution of Nd and Pb isotopes in Central Pacific seawater from ferromanganese crusts. *Earth and Planetary Science Letters*, *146*(1–2), 1–12. https://doi.org/10.1016/s0012-821x(96)00224-5

Little, S. H., Sherman, D. M., Vance, D., & Hein, J. R. (2014). Molecular controls on Cu and Zn isotopic fractionation in Fe-Mn crusts. *Earth and Planetary Science Letters*, *396*, 213–222. https://doi.org/10.1016/j.epsl.2014.04.021

Little, S. H., Vance, D., McManus, J., & Severmann, S. (2016). Key role of continental margin sediments in the oceanic mass balance of Zn and Zn isotopes. *Geology*, *44*(3), 207–210. https://doi.org/10.1130/g37493.1

Little, S. H., Vance, D., Walker-Brown, C., & Landing, W. M. (2014). The oceanic mass balance of copper and zinc isotopes, investigated by analysis of their inputs, and outputs to ferromanganese oxide sediments. *Geochimica Et Cosmochimica Acta*, *125*, 673–693. https://doi.org/10.1016/j.gca.2013.07.046

Maréchal, C. N., Nicolas, E., Douchet, C., & Albarède, F. (2000). Abundance of zinc isotopes as a marine biogeochemical tracer. *Geochemistry, Geophysics, Geosystems*, *1*(5). https://doi.org/10.1029/1999gc000029

Matthews, K. J., Maloney, K. T., Zahirovic, S., Williams, S. E., Seton, M., & Müller, R. D. (2016). Global plate boundary evolution and kinematics since the late Paleozoic. *Global and Planetary Change*, *146*, 226–250. https://doi.org/10.1016/j.gloplacha.2016.10.002

Mavromatis, V., González, A. G., Dietzel, M., & Schott, J. (2019). Zinc isotope fractionation during the inorganic precipitation of calcite - Towards a new pH proxy. *Geochimica et Cosmochimica Acta*, *244*, 99–112. https://doi.org/10.1016/j.gca.2018.09.005

Meynadier, L., Allègre, C., & O'Nions, R. K. (2008). Plate tectonics, radiogenic isotopic tracers and paleoceanography: The case of the manganese crusts in the Pacific. *Earth and Planetary Science Letters*, *272*(3–4), 513–522. https://doi.org/10.1016/j.epsl.2008.04.029

Moore, C. M., Mills, M. M., Arrigo, K. R., Berman-Frank, I., Bopp, L., Boyd, P. W., Galbraith, E. D., Geider, R. J., Guieu, C., Jaccard, S. L., Jickells, T. D., La Roche, J., Lenton, T. M., Mahowald, N. M., Marañón, E., Marinov, I., Moore, J. K., Nakatsuka, T., Oschlies, A., … Ulloa, O. (2013). Processes and patterns of oceanic nutrient limitation. *Nature Geoscience*, *6*(9), 701–710. https://doi.org/10.1038/ngeo1765

Morel, F. M. M., Reinfelder, J. R., Roberts, S. B., Chamberlain, C. P., Lee, J. G., & Yee, D. (1994). Zinc and carbon co-limitation of marine phytoplankton. *Nature*, *369*(6483), 740–742. https://doi.org/10.1038/369740a0

Müller, R. D., Cannon, J., Qin, X. D., Watson, R. J., Gurnis, M., Williams, S., Pfaffelmoser, T., Seton, M., Russell, S. H. J., & Zahirovic, S. (2018). GPlates: Building a Virtual Earth Through Deep Time. *Geochemistry, Geophysics, Geosystems*, *19*(7), 2243–2261. https://doi.org/10.1029/2018gc007584

Neaman, A., Mouélé, F., Trolard, F., & Bourrié, G. (2004). Improved methods for selective dissolution of Mn oxides: applications for studying trace element associations. *Applied Geochemistry*, *19*(6), 973–979. https://doi.org/10.1016/j.apgeochem.2003.12.002

Nielsen, S. G., Mar-Gerrison, S., Gannoun, A., LaRowe, D., Klemm, V., Halliday, A. N., Burton, K. W., & Hein, J. R. (2009). Thallium isotope evidence for a permanent increase in marine organic carbon export in the early Eocene. *Earth and Planetary Science Letters*, *278*(3–4), 297–307. https://doi.org/10.1016/j.epsl.2008.12.010

Norris, R. D., Turner, S. K., Hull, P. M., & Ridgwell, A. (2013). Marine Ecosystem Responses to Cenozoic Global Change. *Science*, *341*(6145), 492–498. https://doi.org/10.1126/science.1240543

Pokrovsky, O. S., Viers, J., & Freydier, R. (2005). Zinc stable isotope fractionation during its adsorption on oxides and hydroxides. *Journal of Colloid and Interface Science*, *291*(1), 192–200. https://doi.org/10.1016/j.jcis.2005.04.079

Shaked, Y., Xu, Y., Leblanc, K., & Morel, F. M. M. (2006). Zinc availability and alkaline phosphatase activity in Emiliania huxleyi: Implications for Zn-P co-limitation in the ocean. *Limnology and Oceanography*, *51*(1), 299–309. https://doi.org/10.4319/lo.2006.51.1.0299

Tribovillard, N., Algeo, T. J., Lyons, T., & Riboulleau, A. (2006). Trace metals as paleoredox and paleoproductivity proxies: An update. *Chemical Geology*, *232*(1–2), 12–32. https://doi.org/10.1016/j.chemgeo.2006.02.012

Wang, X. L., Planavsky, N. J., Reinhard, C. T., Hein, J. R., & Johnson, T. M. (2016). A Cenozoic seawater redox record derived from 238U/235U in ferromanganese crusts. *American Journal of Science*, *316*(1), 64–83. https://doi.org/10.2475/01.2016.02

Weber, T., John, S., Tagliabue, A., & DeVries, T. (2018). Biological uptake and reversible scavenging of zinc in the global ocean. *Science*, *361*(6397), 72–76. https://doi.org/10.1126/science.aap8532

Xiao, K.-Q., Zhao, Y., Liang, C., Zhao, M., Moore, O. W., Otero-Fariña, A., Zhu, Y.-G., Johnson, K., & Peacock, C. L. (2023). Introducing the soil mineral carbon pump. *Nature Reviews Earth & Environment*, *4*(3), 135–136. https://doi.org/10.1038/s43017-023-00396-y

Zachos, J., Pagani, M., Sloan, L., Thomas, E., & Billups, K. (2001). Trends, rhythms, and aberrations in global climate 65 Ma to present. *Science*, *292*(5517), 686–693. https://doi.org/10.1126/science.1059412

Zhang, Y., Planavsky, N. J., Zhao, M., Isson, T., Asael, D., Wang, C., & Wang, F. (2021). The isotopic composition of sedimentary organic zinc and implications for the global Zn isotope mass balance. *Geochimica et Cosmochimica Acta*, *314*, 16–26. https://doi.org/10.1016/j.gca.2021.09.009

Zhao, M. Y., Mills, B. J. W., Homoky, W. B., & Peacock, C. L. (2023). Oxygenation of the Earth aided by mineral-organic carbon preservation. *Nature Geoscience*, *16*(3), 262–267. https://doi.org/10.1038/s41561-023-01133-2

Zhao, M. Y., Tarhan, L. G., Zhang, Y. Y., Hood, A., Asael, D., Reid, R. P., & Planavsky, N. J. (2021). Evaluation of shallow-water carbonates as a seawater zinc isotope archive. *Earth and Planetary Science Letters*, *553*, 116599. https://doi.org/10.1016/j.epsl.2020.116599

Supplementary Materials

Supplementary file

Download: https://ajsonline.org/article/89628-a-cenozoic-record-of-deep-oceanic-zn-isotopic-composition-in-ferromanganese-crusts/attachment/185519.docx